A Quantum Walk Model for Describing the Energy Transfer of a Dressed Photon

M. Ohtsu

Research Origin for Dressed Photon,

3-13-19 Moriya-cho, Kanagawa-ku, Yokohama, Kanagawa 221-0022 Japan

Abstract

This paper presents a quantum walk (QW) model for describing the spatio-temporal behavior of dressed photons (DPs). A three-row vector is used to simultaneously deal with two counter-travelling DPs and a phonon for deriving the probability amplitude of a dressed-photon–phonon (DPP). As the first step, an infinite-sized two-dimensional lattice is assumed to derive spatio-temporal difference equations for this amplitude. Subsequently, a finite-sized two-dimensional lattice is used to install a singularity that serves as an output port. Spatio-temporal difference equations are derived to describe the behavior of the DPP not only inside, but also at the borders and at the corners of the lattice. As the next step, a three-dimensional model is introduced for a more realistic comparison with experimental results. Eighteen combined paths of the DP hopping in the forward-upper and backward-lower directions are regarded as modes 1-18. It is found to be sufficient to study the spatio-temporal behavior of mode 1. Three-dimensional cubes used for this model are transformed to two-dimensional right triangles, and spatio-temporal difference equations are successfully derived.

1. Introduction

Experimental studies on dressed photons (DPs) have been actively carried out and applied to produce a variety of advanced technologies [1-4]. However, one cannot avoid pointing out that theoretical studies are still underdeveloped. The possible reasons for this are: The DP is a quantum field that is created as the result of interaction among multiple elementary particles such as photons and excitons (pairs consisting of electrons and positive holes) in a nanometer-sized complex system. This quantum field is a so-called off-shell field in which the dispersion relation between its momentum and energy is not assigned. Since conventional quantum field theories have dealt only with on-shell fields, they have never provided any theoretical bases for the off-shell field, especially the involvement of light–matter interactions in such a complex system [5]. Although conventional on-shell field studies have employed a perturbation method, it should be pointed out that this method is no more than an emergency treatment for approximately describing the light–matter interactions [6,7].

Fortunately, however, a novel off-shell science theory was built quite recently and succeeded in describing the fundamental process of the interaction for creating the DP [8-13]. To achieve further advances, theories on the spatio-temporal behavior of the DP energy transfer should also be built to

identify the origin of the phenomenon of autonomy that has been experimentally confirmed by the observation of this transfer [14-17]. Although on-shell science has tentatively dealt with the spatio-temporal behavior of the occupation probability of excitons in nanometer-sized particles (NPs) only [18-26], photons and excitons in the complex system must be simultaneously dealt with in order to find a process for constructing a theoretical model for describing the spatio-temporal behavior mentioned above. Furthermore, phonons must be added for describing the dressed-photon–phonon (DPP) that is created as a result of the coupling between the DP and phonons [27].

Employing a quantum walk (QW) model, in which the phonon can be reasonably added [28-30], is one promising theoretical method for simultaneously dealing with these issues. As a first step, this paper describes how to construct a two-dimensional QW model, and as the next step, a three-dimensional model that enables a more realistic comparison with experimental results is discussed.

2. Dressed photon hopping and coupling with phonon

A DP is created in a NP and on its surface if the NP is irradiated by propagating light (wavelength λ) [1]. The size of the DP is equivalent to the size of the NP, and is much smaller than λ. The DP is a quantum field that is created as a result of the interaction among multiple elementary particles such as photons and excitons in a nanometer-sized space [3,4].

The energy of the created DP transfers to the adjacent NP via a process called DP hopping (Fig. 1). In the case where multiple NPs are the atoms in a crystal lattice, the DP excites a lattice vibration during the hopping, resulting in the creation of phonons. Subsequently, the DP exchanges its energy with these phonons to create a DPP quantum field [27].

It should be noted that the DPP cannot be observed from an external macroscopic detection system because its size is still smaller than λ. However, the energy is dissipated when the DPP reaches a singularity (for example, at an impurity atom doped in a crystal (the NP with mass m' in Fig.1) or at the apex of a sharpened fiber probe). The dissipated energy is transformed to propagating light and can be observed by an external detection system. This means that the singularity serves as an output port to create the propagating light that serves as an output signal.

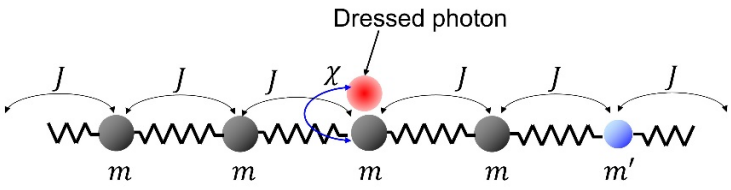

Fig. 1 DP hopping and interaction between the DP and phonons.

m is the mass of the atom of the crystal lattice. m' is that of the impurity atom. J is the hopping constant of the DP. χ is the coupling constant between DP and phonon.

3. Quantum walk model for an infinite-sized two-dimensional lattice

This section discusses the spatio-temporal behavior of the DPP energy transfer in an infinite-sized two-dimensional lattice composed of multiple NPs. In the case of a finite-sized one-dimensional lattice, this behavior has been tentatively analyzed by an on-shell science method [27], and it was demonstrated that the DP travelled in the lattice and was reflected at its end. This means that counter-travelling DPs exist in the lattice as a result of hopping, one traveling to the right and the other to the left. Subsequently, they couple with a phonon to create a DPP.

For analyzing this behavior, this tentative method assigned a system Hamiltonian by summing the DP energy, the phonon energy, the DP-phonon interaction energy for coupling (the coupling constant χ), and the DP hopping energy (the hopping constant J) [1]. It is expected that using the novel QW model presented here can realize higher accuracy in describing this behavior than the tentative method above. In order to construct a QW model for the two-dimensional lattice, the two traveling directions of the DP in the one-dimensional lattice are changed from right/left to the upper-right /lower-left directions, as represented by red and blue broken arrows in Fig. 2(a). While traveling, the DP repeats hopping from one lattice site to its nearest neighbor, as represented by the bent red and blue arrows in this figure. The area around the lattice site represented by a symbol A in Fig. 2(a) is magnified and is shown in Fig. 2(b). The phonon is indicated by the green loop. This loop represents that the phonon is free from the hopping due to its nonlocalized nature. The area around the lattice site represented by a symbol B is magnified and is shown in Fig. 2(c). It should be noted that the directions of the bent red and blue arrows in this figure are different from those in Fig. 2(b).

Since the DPP is a quantum field that is created as a result of coupling between two counter-travelling DPs and a phonon, a three-row vector is used to express its probability amplitude:

$$\vec{\psi}_{t,(x,y)} = \begin{bmatrix} y_{DP+} \\ y_{DP-} \\ y_{Phonon} \end{bmatrix}_{t,(x,y)}, \tag{1}$$

where [ ] represents the vector at time t and at the position of the lattice site (x, y). y_{DP+} and y_{DP-} are the probability amplitudes of the DPs that travel by repeating the hopping in the upper-right (bent red arrows) and lower-left (bent blue arrows) directions, respectively, and y_{Phonon} is that of the phonon. The QW model is more suitable than the random walk model for describing the spatio-temporal behavior of such a vector. Spatial-temporal evolution equations are given separately for Figs. 2(b) and 2(c) by noting that the directions of the bent red and blue arrows in these figures are different from each other.

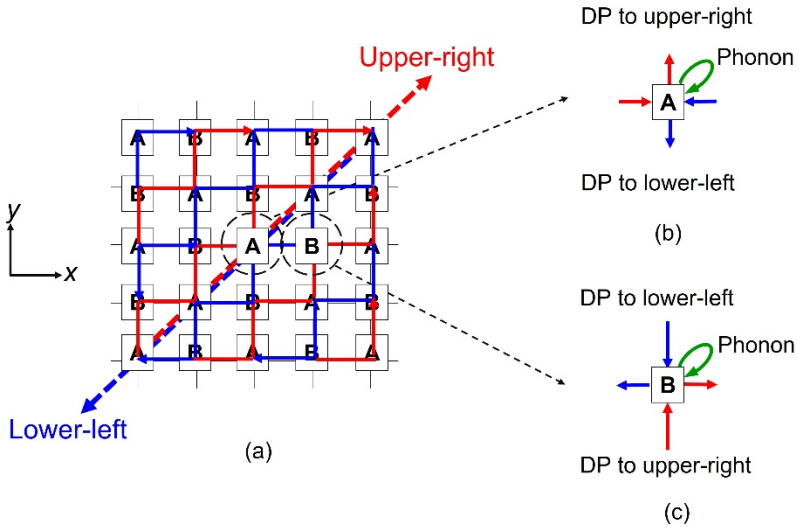

Fig. 2 Two-dimensional lattice.

(a) DP travelling to the upper-right and lower-left (red and blue broken arrows, respectively). The bent red and blue arrows represent the DP hopping from one lattice site to its nearest neighbor, which repeats for these travels. The areas around the lattice sites A and B in (a) are magnified and shown in (b) and (c), respectively. The green loop represents a phonon.

[For the lattice site A] (Fig. 2(b))

The spatial-temporal evolution equation for the vector $\vec{\psi}_{t,(x,y)}$ is given by a difference equation that is represented by

$$\vec{\psi}_{t+1,(x,y)} = P_{+}\vec{\psi}_{t,(x-1,y)} + P_{-}\vec{\psi}_{t,(x+1,y)} + P_{0}\vec{\psi}_{t,(x,y)}\,. \tag{2}$$

It should be noted that the positions of the sites represented by the first and second terms on the right-hand side are $(x-1, y)$ and $(x+1, y)$, respectively, because the DPs hopping to the upper-right (bent red arrow) and lower-left (bent blue arrow) positions originate in the left and right neighboring sites of the site A, respectively.

The three matrices on the right-hand side are

$$P_{+} = \begin{bmatrix} \varepsilon_{+} & J & \chi \\ 0 & 0 & 0 \\ 0 & 0 & 0 \end{bmatrix}, \tag{3a}$$

$$P_{-}=\begin{bmatrix}0 & 0 & 0\\ J & \varepsilon_{-} & \chi\\ 0 & 0 & 0\end{bmatrix}, \tag{3b}$$

and

$$P_{0}=\begin{bmatrix}0 & 0 & 0\\ 0 & 0 & 0\\ \chi & \chi & \varepsilon_{0}\end{bmatrix}. \tag{3c}$$

Diagonal elements ε_{+} and ε_{-} in eqs. (3a) and (3b) are the eigen-energies of the DPs that travel to the upper-right and lower-left positions, respectively, and ε_{0} in eq. (3c) is that of the phonon. The roles of off-diagonal elements χ and J are:

1) The value of $y_{DP+,t+1,(x,y)}$ (the first row of the vector $\vec{\psi}_{t+1,(x,y)}$; hops to the upper-right) on the left-hand side of eq. (2) is given by the first term on the right-hand side, in which J and χ of P_{+} represent the magnitudes of the contributions of the DP ($y_{DP-,t,(x-1,y)}$) that hops to the lower-left position and that of the interaction with the phonon ($y_{Phonon,t,(x-1,y)}$), respectively.

2) The value of $y_{DP-,t+1,(x,y)}$ (the second row of the vector $\vec{\psi}_{t+1,(x,y)}$; hops to the lower-left) on the left-hand side of eq. (2) is given by the second term on the right-hand side, in which J and χ of P_{-} represents the magnitudes of the contributions of the DP ($y_{DP+,t,(x+1,y)}$) that hops to the upper-right position and that of the interaction with the phonon ($y_{Phonon,t,(x+1,y)}$), respectively.

3) The value of $y_{Phonon,t+1,(x,y)}$ (the third row of the vector $\vec{\psi}_{t+1,(x,y)}$) in the left-hand side of eq. (2) is given by the third term on the right-hand side, in which the two χ s of P_{0} represent the magnitudes of the contributions of the phonon that interacts with the counter-travelling DPs ($y_{DP+,t,(x,y)}$ and $y_{DP-,t,(x,y)}$).

[For the lattice site B] (Fig. 2(c))

The spatial-temporal evolution equation is

$$\vec{\psi}_{t+1,(x,y)} = P_+\vec{\psi}_{t,(x,y-1)} + P_-\vec{\psi}_{t,(x,y+1)} + P_0\vec{\psi}_{t,(x,y)} . \tag{4}$$

It should be noted that the sites for the first and second terms on the right-hand side are $(x, y-1)$ and $(x, y+1)$, respectively, because the DPs hopping to the upper-right (red arrow) and lower-left (blue arrow) positions originate in the lower and upper neighbor sites of the site B, respectively. The roles of off-diagonal elements χ and J are equivalent to those in 1) – 3) above for the lattice site A.

By summing the three matrices of eqs. (3a) – (3c), one has

$$U = P_+ + P_- + P_0 = \begin{bmatrix} \varepsilon_+ & J & \chi \\ J & \varepsilon_- & \chi \\ \chi & \chi & \varepsilon_0 \end{bmatrix}, \tag{5}$$

which meets a unitarity requirement for the QW model. This is because, as an example, this matrix can be set to

$$U = \begin{bmatrix} \varepsilon_+ & J & \chi \\ J & \varepsilon_- & \chi \\ \chi & \chi & \varepsilon_0 \end{bmatrix} = \begin{bmatrix} -\cos^2\theta & \sin^2\theta & \dfrac{\sin 2\theta}{\sqrt{2}} \\ \sin^2\theta & -\cos^2\theta & \dfrac{\sin 2\theta}{\sqrt{2}} \\ \dfrac{\sin 2\theta}{\sqrt{2}} & \dfrac{\sin 2\theta}{\sqrt{2}} & \cos 2\theta \end{bmatrix}, \tag{6}$$

which is exactly a unitary matrix.

As the first step of numerical calculation, one can assume $\chi = J$ for simplicity, indicating that the DP-phonon interaction energy is equal to the DP hopping energy. This assumption can be represented by setting the value of θ to $\sin^{-1}\sqrt{2/3}$, which leads to

$$U = \begin{bmatrix} \varepsilon_+ & J & \chi \\ J & \varepsilon_- & \chi \\ \chi & \chi & \varepsilon_0 \end{bmatrix} = \begin{bmatrix} -\dfrac{1}{3} & \dfrac{2}{3} & \dfrac{2}{3} \\ \dfrac{2}{3} & -\dfrac{1}{3} & \dfrac{2}{3} \\ \dfrac{2}{3} & \dfrac{2}{3} & -\dfrac{1}{3} \end{bmatrix}. \tag{7}$$

The relation $\chi > J$ indicates that the DP-phonon interaction energy is larger than the DP hopping energy. In this case, the possibility of the DPP creation is larger than that of the case $\chi < J$. Thus, a larger value of the probability $\left|\vec{\psi}_{t,(x,y)}\right|^2$ is expected at the output port, creating a larger output signal when the DPP energy dissipates. In the case of $\chi > J$ or $\chi < J$, the value of θ can be set to $\theta < \sin^{-1}\sqrt{2/3}$ or $\theta > \sin^{-1}\sqrt{2/3}$, respectively[1)].

For the numerical calculation, eqs. (3) or (4) is selectively used depending on whether the DP is at site A or B at t and (x, y). Random numbers can be used for this selection.

---

1) Equation (6) indicates that $\varepsilon_+ + \varepsilon_- + \varepsilon_0$ takes a constant value (-1), which means that the total energy is conserved and is independent of the value of θ. The negative value -1 originates from the fact that the two-dimensional lattice under consideration (Fig. 2) is an open system that accepts the input signal (the irradiated propagating light for DP creation). Thus, by adding the input signal energy if necessary, the total energy becomes a positive value.

---

4. Quantum walk model for a finite-sized two-dimensional lattice

In order to experimentally evaluate the spatio-temporal behavior of the DPP energy transfer in the lattice, the magnitude of the energy dissipated at the output port has been observed by an external macroscopic detection system [1-4]. The propagating light created at the output port has been used as an output signal for this observation.

As was described at the end of Section 2, since a singularity corresponds to the output port, the size of the two-dimensional lattice must be finite to install this singularity inside, at the border, or at the corner of the lattice. Figure 3 schematically explains such a finite-sized two-dimensional lattice to be considered in this section. Since the directions of the bent red arrows passing through the sites A and B in Figs. 2(b) and (c) are opposite to each other (those of the bent blue arrows were also opposite), this section uses a six-row vector that is expressed as

$$\vec{\psi}_{t,(x,y)} = \begin{bmatrix} \vec{\psi}^{\Leftrightarrow} \\ \vec{\psi}^{\Updownarrow} \end{bmatrix}_{t,(x,y)} . \tag{8}$$

It can be given by two three-row vectors, as was the case of eq. (1). They are

$$\vec{\psi}^{\Leftrightarrow}_{t,(x,y)} = \begin{bmatrix} y^{\Leftrightarrow}_{DP+} \\ y^{\Leftrightarrow}_{DP-} \\ y^{\Leftrightarrow}_{Phonon} \end{bmatrix}_{t,(x,y)} \tag{9a}$$

and

$$\vec{\psi}^{\Updownarrow}_{t,(x,y)} = \begin{bmatrix} y^{\Updownarrow}_{DP+} \\ y^{\Updownarrow}_{DP-} \\ y^{\Updownarrow}_{Phonon} \end{bmatrix}_{t,(x,y)} . \tag{9b}$$

The double-pointed arrows $\Leftrightarrow$ and $\Updownarrow$ represent the DP hopping along the x- and y-axes, respectively (Fig. 4). For the sake of consistent expressions, these arrows are also used for the phonon (the third rows in eqs. (9a) and (9b)) even though the phonon does not hop.

In the following parts of this section, the spatio-temporal evolution equations for the vector (eqs. (9a) and (9b)) inside, at the borders, and at the corners of the lattice are derived.

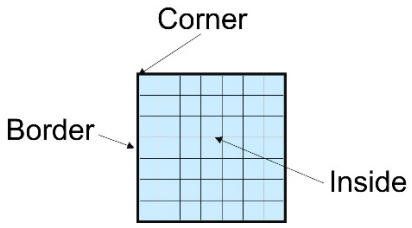

Fig. 3 A finite-sized two-dimensional lattice.

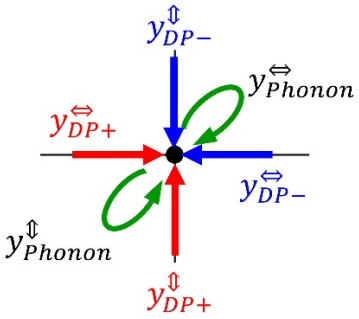

Fig. 4 Schematic explanation of the double-pointed arrows $\Leftrightarrow$ and $\Updownarrow$.

4.1 Inside the lattice

When the DP is inside the lattice (Fig. 5), the bent red and blue arrows in Fig. 2 indicate that the DP hops along the x- ($\Leftrightarrow$) and y- ($\Updownarrow$) axes alternately. Thus, the spatio-temporal evolution equations are given by

$$\vec{\psi}^{\Leftrightarrow}_{t+1,(x,y)} = P^{\Updownarrow}_{+}\vec{\psi}^{\Updownarrow}_{t,(x-1,y)} + P^{\Updownarrow}_{-}\vec{\psi}^{\Updownarrow}_{t,(x+1,y)} + P^{\Updownarrow}_{0}\vec{\psi}^{\Updownarrow}_{t,(x,y)} \tag{10a}$$

and

$$\vec{\psi}^{\Updownarrow}_{t+1,(x,y)} = P^{\Leftrightarrow}_{+}\vec{\psi}^{\Leftrightarrow}_{t,(x,y-1)} + P^{\Leftrightarrow}_{-}\vec{\psi}^{\Leftrightarrow}_{t,(x,y+1)} + P^{\Leftrightarrow}_{0}\vec{\psi}^{\Leftrightarrow}_{t,(x,y)}, \tag{10b}$$

where $P^{\Leftrightarrow}_{+} = P^{\Updownarrow}_{+}$, $P^{\Leftrightarrow}_{-} = P^{\Updownarrow}_{-}$, and $P^{\Leftrightarrow}_{0} = P^{\Updownarrow}_{0}$ are equal to P_{+}, P_{-}, and P_{0} of eqs. (3a) - (3c), respectively. For the numerical calculation, eqs. (10a) and (10b) are alternatively used to derive the value of $\left|\vec{\psi}_{t,(x,y)}\right|^2$ from eq. (8). Random numbers can be also used if necessary.

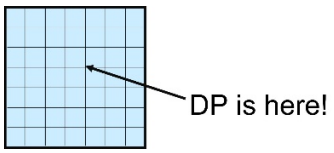

Fig. 5 Inside the lattice.

4.2 At the border

For dealing with the DP at the left border of the lattice (Fig. 6), a matrix

$$\sigma = \begin{bmatrix} 0 & 1 & 0 \\ 1 & 0 & 0 \\ 0 & 0 & 1 \end{bmatrix} \tag{11}$$

is introduced to represent the reflection of y_{DP-} that hops along the -*x* axis and is normally incident at this border. By using this matrix, y_{DP-} given by the first term on the right-hand side of eq. (10a) is replaced by y_{DP+} and is expressed as

$$\vec{\psi}^{\Leftrightarrow}_{t+1,(x,y)} = \sigma P^{\Updownarrow}_{-}\vec{\psi}^{\Updownarrow}_{t,(x,y)} + P^{\Updownarrow}_{-}\vec{\psi}^{\Updownarrow}_{t,(x+1,y)} + P^{\Updownarrow}_{0}\vec{\psi}^{\Updownarrow}_{t,(x,y)}. \tag{12a}$$

For deriving $\vec{\psi}^{\Updownarrow}_{t+1,(x,y)}$ at this border, eq. (10b) can also be used because y_{DP+} and y_{DP-}, hopping along the +*y*- and -*y*-axes, are not incident on the border:

$$\vec{\psi}^{\Updownarrow}_{t+1,(x,y)} = P^{\Leftrightarrow}_{+}\vec{\psi}^{\Leftrightarrow}_{t,(x,y-1)} + P^{\Leftrightarrow}_{-}\vec{\psi}^{\Leftrightarrow}_{t,(x,y+1)} + P^{\Leftrightarrow}_{0}\vec{\psi}^{\Leftrightarrow}_{t,(x,y)}. \tag{12b}$$

Figures 7(a) and (b) schematically explain the roles of each term on the right-hand side of these equations. Figure 8 summarizes the reflection at four borders of the lattice. For the numerical calculation, eqs. (12a) and (12b) are alternatively used to derive the value of $\left|\vec{\psi}_{t,(x,y)}\right|^2$ from eq. (8).

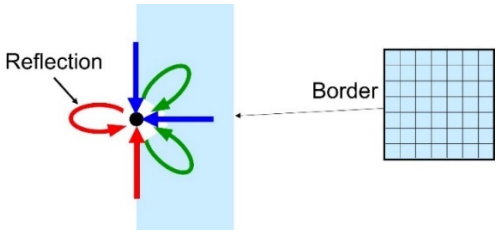

Fig. 6 Reflection at the left border.

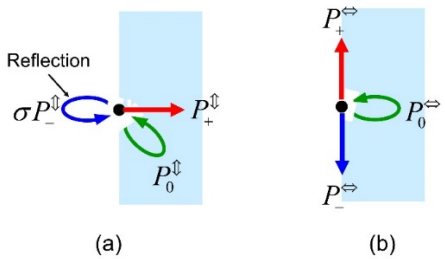

Fig. 7 Schematic explanation of the roles of each term of the right-hand side of eqs. (12a) and (b).

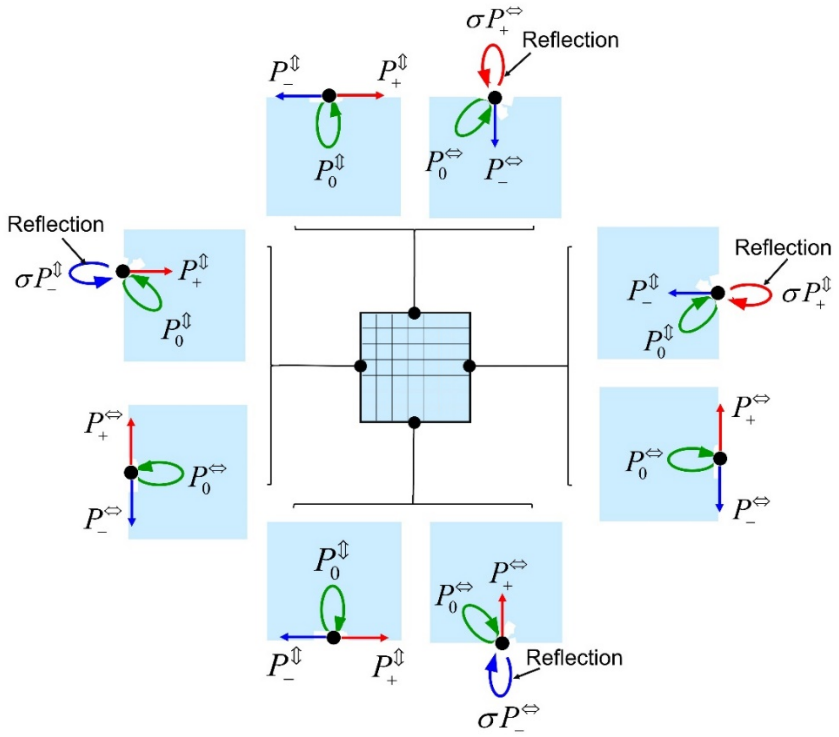

Fig. 8 Schematic explanation of the reflection at four borders of the lattice.

4.3 At the corner

Figure 9 schematically explains the reflection at four corners of the lattice. Since the corner X in this figure is the point of intersection of the left and upper borders, spatio-temporal evolution equations for the left and upper borders in Section 4.2 can be used at this corner. Equation (12a) is used for the left border, that is, by referring to the discussion in Section 4.2,

$$\vec{\psi}^{\Leftrightarrow}_{t+1,(x,y)} = \sigma P^{\Updownarrow}_{-}\vec{\psi}^{\Updownarrow}_{t,(x,y)} + P^{\Updownarrow}_{-}\vec{\psi}^{\Updownarrow}_{t,(x+1,y)} + P^{\Updownarrow}_{0}\vec{\psi}^{\Updownarrow}_{t,(x,y)} . \tag{13a}$$

The equation for the upper border is

$$\vec{\psi}^{\Updownarrow}_{t+1,(x,y)} = \sigma P^{\Leftrightarrow}_{+}\vec{\psi}^{\Leftrightarrow}_{t,(x,y)} + P^{\Leftrightarrow}_{-}\vec{\psi}^{\Leftrightarrow}_{t,(x,y-1)} + P^{\Leftrightarrow}_{0}\vec{\psi}^{\Leftrightarrow}_{t,(x,y)} . \tag{13b}$$

It should be pointed out that $P^{\Leftrightarrow}_{+}\vec{\psi}^{\Leftrightarrow}_{t,(x,y-1)}$, the first term of eq. (12b), was replaced by $\sigma P^{\Leftrightarrow}_{+}\vec{\psi}^{\Leftrightarrow}_{t,(x,y)}$ in eq. (13b) in order to represent the reflection at the upper border. It should also be noted that the second term was changed from $P^{\Leftrightarrow}_{-}\vec{\psi}^{\Leftrightarrow}_{t,(x,y+1)}$ - to $P^{\Leftrightarrow}_{-}\vec{\psi}^{\Leftrightarrow}_{t,(x,y-1)}$ because the site at the position $(x, y+1)$ is beyond the border.

Spatio-temporal evolution equations for the other corners in Fig. 9 are similar to eqs. (13a) and (13b) and can be derived by a method equivalent to that above.

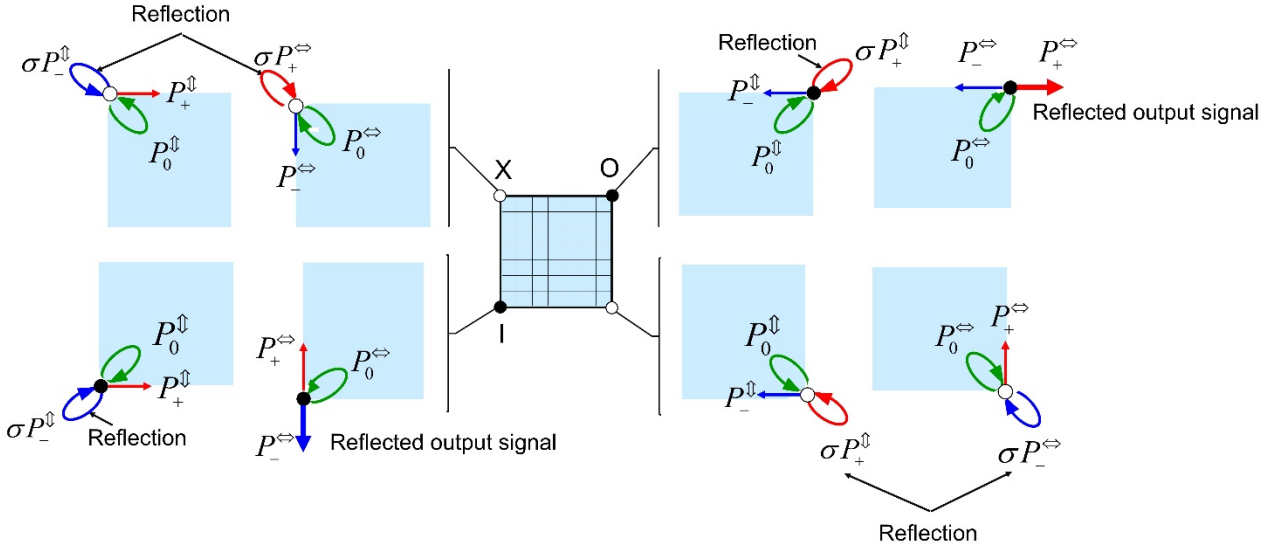

Fig. 9 Schematic explanation of the reflection at four corners of the lattice.

4.4 At the input and output ports

At the input port $(x, y) = (0, 0)$ (at the corner I in Fig. 9), one can set

$$\vec{\psi}^{\Leftrightarrow}_{t,(0,0)} = \begin{bmatrix} y^{\Leftrightarrow}_{DP+} \\ y^{\Leftrightarrow}_{DP-} \\ y^{\Leftrightarrow}_{Phonon} \end{bmatrix}_{t,(0,0)} = \begin{bmatrix} 0 \\ 0 \\ 0 \end{bmatrix} \tag{14a}$$

and

$$\vec{\psi}^{\Updownarrow}_{t,(0,0)} = \begin{bmatrix} y^{\Updownarrow}_{DP+} \\ y^{\Updownarrow}_{DP-} \\ y^{\Updownarrow}_{Phonon} \end{bmatrix}_{t,(0,0)} = \begin{bmatrix} a(t) \\ 0 \\ 0 \end{bmatrix}. \tag{14b}$$

In the case of a constant intensity input signal, $a(t)$ can be fixed to unity.

The first example of the output port is the NP with mass m' in Fig. 1, which is installed inside the lattice (the impurity atom). In this case, the value of χ must be set larger than that of J because experimental studies have confirmed that the DP more likely localizes at the impurity atom than at the host crystal atom. The second example is the apex of a fiber probe that corresponds to the corner O in Fig. 9. The values of the $\left|\vec{\psi}_{t,(x,y)}\right|^2$ in eq. (8) at these output ports are used to evaluate the output signal intensity.

The aim of the numerical calculation is to find the travelling path of the DP that maximizes the value of $\left|\vec{\psi}_{t,(x,y)}\right|^2$ at the output port, and to identify the origin of the autonomy in the DP energy transfer, as was described in Section 1 [14-17].

5 Evolution to a three-dimensional lattice

This section derives the spatio-temporal evolution equations in the infinite-sized three-dimensional lattice of Fig. 10 for constructing a three-dimensional QW model. Red and blue broken arrows in this figure represent the three-dimensional counter-travelling DP in the forward-upper $(+x, +y, +z)$ and backward-lower $(-x, -y, -z)$ directions, respectively. All three-dimensional lattice sites are numbered (1-27) for the discussion below.

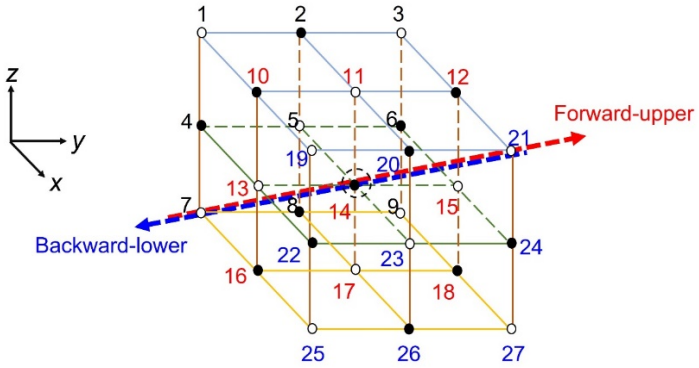

Fig. 10 Three-dimensional lattice.

5.1 Modes of DP hopping

Instead of bent red and blue arrows in the two-dimensional lattice (Fig. 2(a)), three-dimensionally bent arrows are assumed, as shown in Figs. 11 and 12, respectively. Site 14 at the center of Fig. 10 is selected as the starting point of the three-dimensional DP hopping. Figure 11 represents six possible paths (F-L1—F-R3) of the DP that hops in the forward-upper direction from site 14 to site 21. After leaving site 14, the red arrows in F-L1, F-L2, and F-L3 advance like a left-handed (L) screw to reach site 21. In contrast, the arrows in F-R1, F-R2, and F-R3 advance like a right-handed (R) screw. Figure 12 represents six possible paths (B-L1—B-R3) of the DP hopping in the backward-lower direction from site 14 to site 7. The bent blue arrows in B-L1, B-L2, and B-L3 advance like a left-handed (L) screw to reach site 7. In contrast, the arrows in B-R1, B-R2, and B-R3 advance like a right-handed (R) screw.

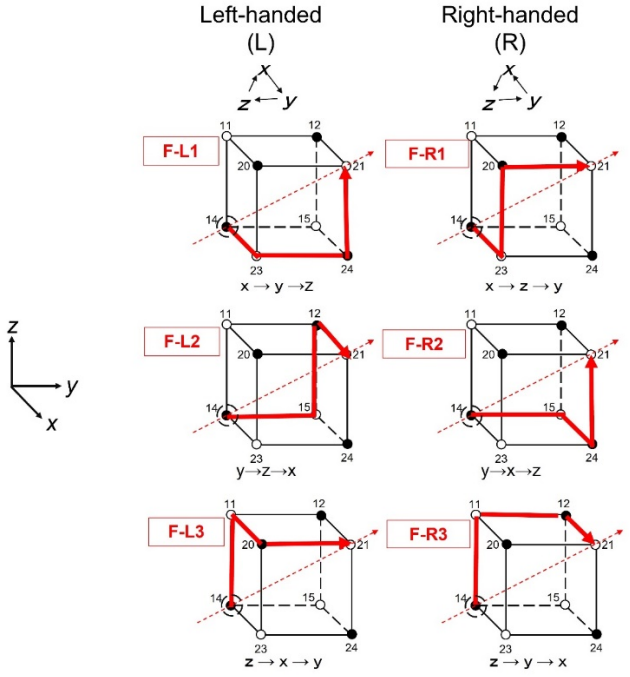

Fig. 11 DP hopping toward the forward-upper direction.

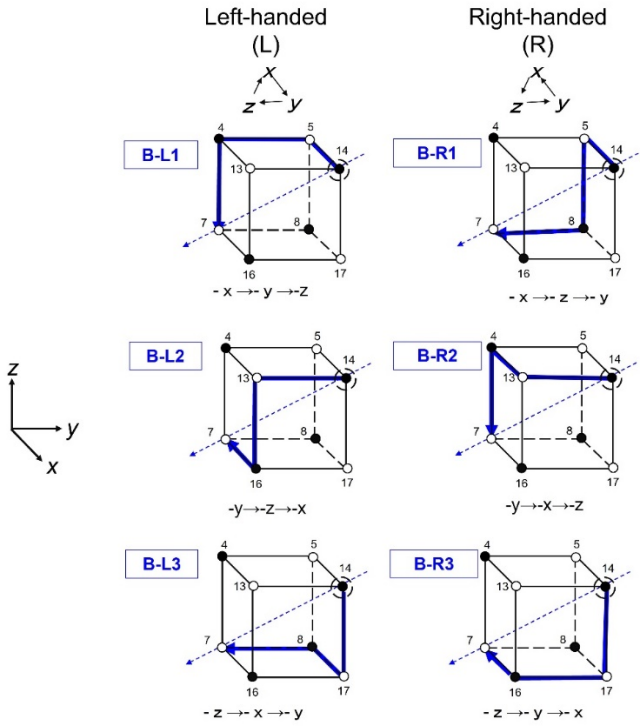

Fig. 12 DP hopping toward the backward-lower direction.

By expressing the matrices representing the ± 90 degree-rotation around the *x*-, *y*-, and *z*-axes, respectively, as

$$\Theta_{\pm x} = \begin{bmatrix} 1 & 0 & 0 \\ 0 & 0 & \pm 1 \\ 0 & \mp 1 & 0 \end{bmatrix}, \tag{15a}$$

$$\Theta_{\pm y} = \begin{bmatrix} 0 & 0 & \mp 1 \\ 0 & 1 & 0 \\ \pm 1 & 0 & 0 \end{bmatrix}, \tag{15b}$$

and

$$\Theta_{\pm z} = \begin{bmatrix} 0 & \mp 1 & 0 \\ \pm 1 & 0 & 0 \\ 0 & 0 & 1 \end{bmatrix}, \tag{15c}$$

the first row in each column of Figs. 11 and 12 is transformed to the second row by the operation $\Theta_{-y}\Theta_{z}$, and from the second to the third rows by $\Theta_{z}\Theta_{-x}$. These operations are represented by the matrix

$$R_{\Theta} = \Theta_{-y}\Theta_{z} = \Theta_{z}\Theta_{-x} = \begin{bmatrix} 0 & 0 & 1 \\ 1 & 0 & 0 \\ 0 & 1 & 0 \end{bmatrix}, \tag{16}$$

which indicates the operation of rotating the (x, y, z)-axis to the (z, x, y)-axes. By combining the six bent red (F-L1 – F-R3) and blue (B-L1 – B-R3) arrows in Figs. 11 and 12, one can form thirty-six paths of the DP hopping in the forward-upper and backward-lower directions. Among them, eighteen combinations are physically acceptable: they are represented by 1–18 in Table 1. Figure 13 schematically explains the paths in these combinations. It can be confirmed that the paths of the red and blue arrows in combinations 1–18 do not overlap with each other in the two cubes during the screw-like advancing motion. The other eighteen combinations are not acceptable because some of their paths overlap with each other.

Table 1 Acceptable combinations.

	B-L1	B-L2	B-L3	B-R1	B-R2	B-R3
F-L1	1			2	3	
F-L2		4			5	6
F-L3			7	8		9
F-R1	10		11	12		
F-R2	13	14			15	
F-R3		16	17			18

These combinations 1-18 can be regarded as the modes of DP hopping and can be grouped as follows:

Group 1: Modes 1, 4, and 7. Group 2: Modes 2, 5, and 9.

Group 3: Modes 10, 14, and 17. Group 4: Modes 3, 6, and 8.

Group 5: Modes 11, 13, and 16. Group 6: Modes 12, 15, and 18.

Furthermore, by exchanging the bent red and blue arrows after the rotation operation, groups 1, 2, and 3 are transformed to groups 6, 4, 5, respectively. This transformation indicates that these groups form three pairs: [groups 1 and 6], [groups 2 and 4], and [groups 3 and 5]. Thus, the groups, being independent of each other, are found to be the groups 1, 2, and 3.

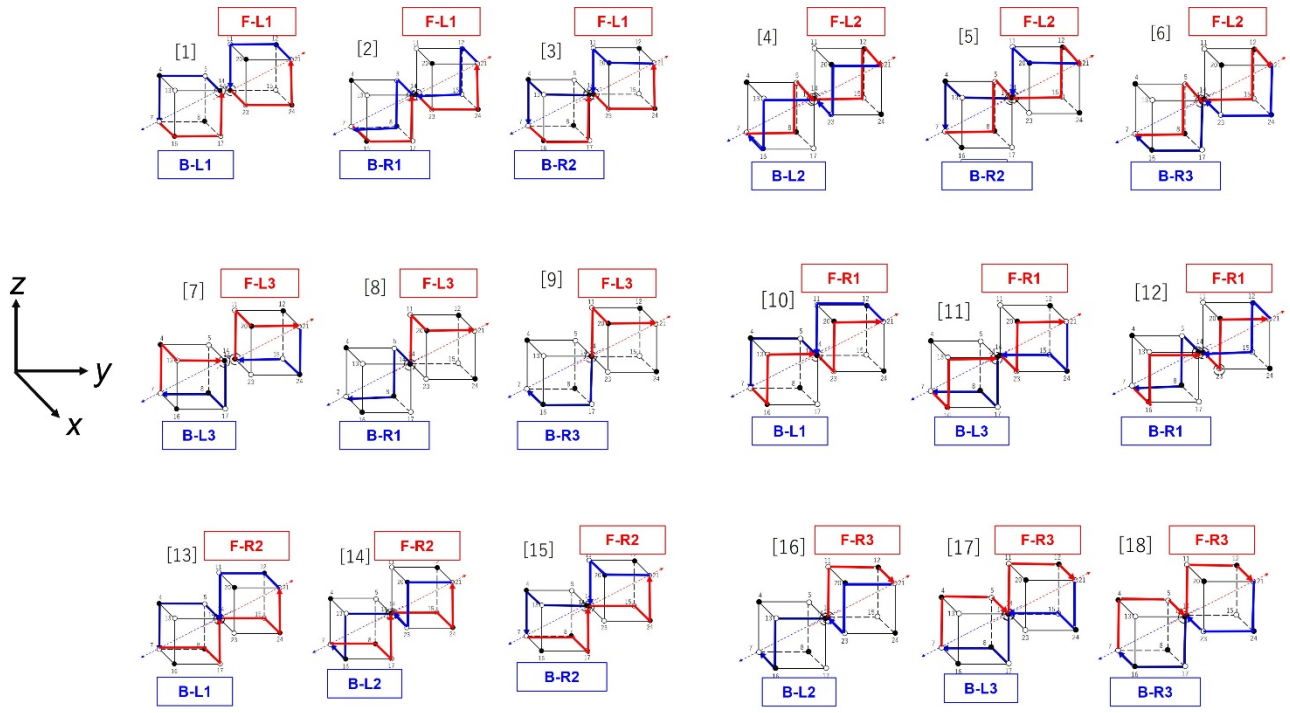

Fig. 13 Paths in the combinations 1 - 18.

The reasons why this grouping and pairing are possible are that the (x, y, z)-axes between these modes can be exchanged by repeating the rotation operation R_{Θ}.

Since the representative modes of the groups 1, 2, and 3 above are 1, 2, and 10, respectively, the behavior of the three-dimensional DP hopping can be fully described if the spatio-temporal evolution equations for these three modes can be derived. This is because rotational symmetry and inversion symmetry are guaranteed in the infinite-sized three-dimensional lattice.

For these modes, the site numbers and the positions of the tails of the red and blue arrows that hop to site 14, are, respectively,:

Mode 1: Red arrow: site number 17, position of the tail $(x, y, z-1)$,

Blue arrow: site number 11, position of the tail $(x, y, z+1)$,

Mode 2: Red arrow: site number 17, position of the tail $(x, y, z-1)$,

Blue arrow: site number 15, position of the tail $(x, y+1, z)$,

Mode 10: Red arrow: site number 13, position of the tail $(x, y-1, z)$,

Blue arrow: site number 11, position of the tail $(x, y, z+1)$.

When the DP at site 14 subsequently hops to the nearest neighbor site and reaches site 21 or 7, a cycle of the three-dimensional hopping is completed. By repeating this hopping, the travelling in the forward-upper and backward-lower directions, as represented by red and blue broken arrows in Fig. 10, is realized.

It should be pointed out that it is sufficient to study mode 1 because modes 2 and 10 above cannot be used for the QW model[2)].

2) In modes 2 and 10, the bent red arrow has two paths when it flows in and out of site 5. Furthermore, the bent blue arrow also has two paths when it flows in and out of site 23. If these paths are included, the matrices in the evolution equations are not unitary. Thus, modes 2 and 10 do not meet the requirement for the QW model.

5.2 Spatio-temporal evolution equations

For deriving evolution equations, the eight vertices of the cubes in Figs. 11 and 12 are represented by four symbols A, B, C, and D, as shown by Fig. 14, in order to represent that the two vertices on the diagonal line of the cube are identical. As a result of this identification, three-dimensional cubes in Figs. 14(a) and (b) can be transformed to two-dimensional right triangles, as shown by Figs. 15(a) and (b). The symbols $\pm x$, $\pm y$, and $\pm z$ represent the directions of the bent red (y_{DP+}) and blue (y_{DP-}) arrows. It should be noted that the vertex D is isolated from these triangles. As a result of this transformation, the directions of the bent red and blue arrows in Figs. 15(a) and (b) are made parallel to each other, forming a counterclockwise loop. However, the signs of x, y, and z for these red and blue arrows are opposite to each other, indicating the counter-travelling of the DPs. Figure 15(c) is derived by superposing Figs. 15(a) and (b).

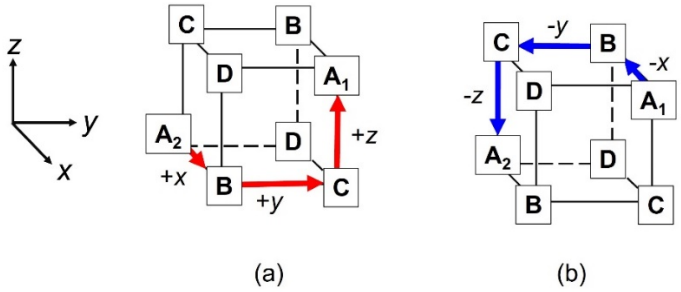

Fig. 14 The directions of the bent red (y_{DP+}) and blue (y_{DP-}) arrows in a three-dimensional cube.

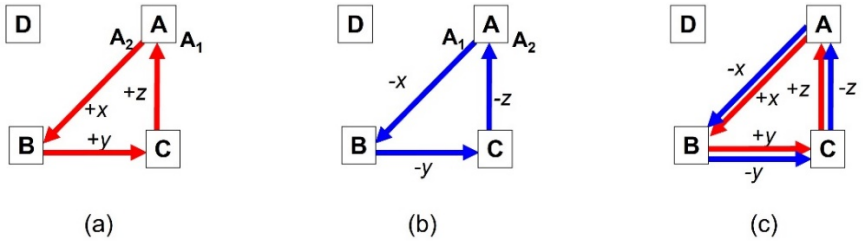

Fig. 15 Transformed to two-dimensional right triangles from which the vertex D is isolated.
(a) and (b) are for the bent red and blue arrows, respectively. (c) is the figure derived by superposing (a) and (b).

Horizontal red and blue arrows ($\rightarrow$ and $\rightarrow$) on the base of the right triangle in Figs. 15(a)-(c) correspond to $y_{DP+}^{\Leftrightarrow}$ and $y_{DP-}^{\Leftrightarrow}$ of eq. (9a), respectively. Vertical arrows ($\uparrow$ and $\uparrow$) are $y_{DP+}^{\Updownarrow}$ and $y_{DP-}^{\Updownarrow}$ of eq. (9b). It should be noted that there are additional red and blue arrows on the hypotenuse of the right triangle, being different from the two-dimensional lattice of Section 3.1. Finally, Fig. 16 is derived by adding green loops in order to include the contribution of the phonon (y_{Phonon} of eq.(1)).

By referring to Fig. 16, the spatio-temporal evolution equations are derived and expressed as

[For site A]

$$\vec{\psi}_{t+1,(x,y,z)} = P_{+}\vec{\psi}_{t,(x,y,z-1)} + P_{-}\vec{\psi}_{t,(x,y,z+1)} + P_{0}\vec{\psi}_{t,(x,y,z)}, \tag{17a}$$

[For site B]

$$\vec{\psi}_{t+1,(x,y,z)} = P_{+}\vec{\psi}_{t,(x-1,y,z)} + P_{-}\vec{\psi}_{t,(x+1,y,z)} + P_{0}\vec{\psi}_{t,(x,y,z)}, \tag{17b}$$

[For site C]

$$\vec{\psi}_{t+1,(x,y,z)} = P_{+}\vec{\psi}_{t,(x,y-1,z)} + P_{-}\vec{\psi}_{t,(x,y+1,z)} + P_{0}\vec{\psi}_{t,(x,y,z)}, \tag{17c}$$

and

[For site D]

$$\vec{\psi}_{t+1,(x,y,z)} = P_{0}\vec{\psi}_{t,(x,y,z)}. \tag{17d}$$

For numerical calculations to derive the value of $\left|\vec{\psi}_{t,(x,y)}\right|^2$ from eq. (8), one of eqs. (17a) - (17d) is selected and used depending on at which site the DP stays at t. Random numbers can be used for this selection. For a finite-sized three-dimensional lattice, spatio-temporal evolution equations can be derived by using the matrix σ in eq. (11) to include the effect of reflection at the border or the corner.

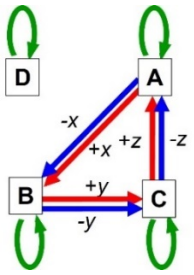

Fig. 16 Closed-loops that represent the contribution of phonons.

6. Summary

This paper presented a quantum walk (QW) model for describing the spatio-temporal behavior of the dressed photon (DP). Since a dressed-photon–phonon (DPP) is created as a result of coupling between the two counter-travelling DPs and a phonon, a three-row vector was used to simultaneously deal with them for deriving the probability amplitude of the DPP.

As the first step, an infinite-sized two-dimensional lattice was assumed in order to derive spatio-temporal difference equations. It was confirmed that the sum of the three matrices in these equations met the unitarity requirement for the QW model. Subsequently, a finite-sized two-dimensional lattice was assumed to install a singularity that serves as the output port. Spatio-temporal difference equations were derived to describe the behavior of the DPP not only inside, but also at the borders and at the corners of the lattice. At the border, an additional matrix was introduced to represent the reflection of the DP. At the output port installed at the corner, the values of the probability amplitude above were used to evaluate the output signal intensity.

As the next step, a three-dimensional model was discussed to enable a more realistic comparison with experimental results. Eighteen combined paths of the DP hopping in forward-upper and backward-lower directions were regarded as modes 1-18 of DP hopping, which were grouped into six groups. Finally, it was found to be sufficient to study the spatio-temporal behavior of mode 1. A three-dimensional cube used for this model was transformed to two-dimensional right triangles, and spatio-temporal difference equations were successfully derived.

To make further progress in these studies, a finite-sized three-dimensional lattice should be investigated for describing the behavior of the DP at the border or the corner. By doing so, it is expected that the value of the probability amplitude at the output port can be numerically calculated, and the origin of the autonomy in the DP energy transfer can be identified. Furthermore, it is expected that the results of these numerical calculations can be used as design criteria for advanced experimental systems.

Acknowledgements

The author thanks Prof. E. Segawa (Yokohama National University) for his painstaking guidance on the QW model, especially for proposing the formulation methods described in Sections 3, 4, and 5.2. He also thanks Dr. K. Yuki (Analytics Japan Co., Ltd.) for actively carrying out numerical calculations of the two-dimensional QW model to be published elsewhere.

References

[1] Ohtsu, M. (2013). *Dressed Photons*; Springer-Verlag, Heidelberg, November 2013.

[2] Ohtsu, M. (2013). *Silicon Light-Emitting Diodes and Lasers*; Springer-Verlag, Heidelberg, August 2016.

[3] Ohtsu, M.(2018). Historical Review of Dressed Photons: Experimental Progress and Required Theories. *Progress in Nanophotonics 5*, ed. by T. Yatsui, Springer, Heidelberg, October 2018, 1-51.

[4] Ohtsu, M. (2020). History, current development, and future directions of near-field optical science. *Opto-Electronic Advances*, 3, no.3, 190046. DOI: 10.29026/oea.2020.190046

[5] Streater, R.F. & Wightman, A.S. (1964). *PCT, Spin and Statistics, and All That.*; (pp.163-165). Princeton: Princeton Univ. Press.

[6] Kobayashi, K. & Ohtsu, M. (1999). Quantum theoretical approach to a near-field optical system. *Journal of Microscopy*, *194*, 249-254.

[7] Sangu, S., Kobayashi, K., & Ohtsu, M. (2001). Optical near fields as photon-matter interacting systems. *J. Microscopy*, *202*, 279-285.

[8] Ohtsu, M., Ojima, I., and Sakuma, H. (2019). Dressed Photon as an Off-Shell Quantum Field. *Progress in Optics 64*, ed.by T. D. Visser, Elsevier, Amsterdam, 45-97.

[9] Sakuma, H., Ojima, I., and Ohtsu, M. (2017). Dressed photons in a new paradigm of off-shell quantum fields. *Progress in Quantum Electronics*, **55**, 74-87.

[10] Sakuma, H., Ojima, I., and Ohtsu, M. (2017). Gauge symmetry breaking and emergence of Clebsch-dual electromagnetic field as a model of dressed photons. *Appl. Phys.*A, **123**:750.

[11] Sakuma, H. (2018). Virtual Photon Model by Spatio-Temporal Vortex Dynamics. *Progress in Nanophotonics 5*, ed. by T. Yatsui, Springer, Heidelberg, 53-77.

[12] Sakuma, H., Ojima, I., Ohtsu, M., and Ochiai, H. (2020). Off-Shell Quantum Fields to Connect Dressed Photons with Cosmology. *Symmetry*, **12**, 1244-1263. DOI:10.3390/sym12081244

[13] Sakuma, H. & Ojima, I. (2021). On the Dressed Photon Constant and Its Implication for a Novel Perspective on Cosmology. *Symmetry* **13**, 593. https://doi.org/10.3390/sym13040593

[14] Ohtsu, M., Kawazoe, T., & Saigo, H. (2017). Spatial and Temporal Evolutions of Dressed Photon Energy Transfer. *Off-shell Archive,* Offshell:1710R.001.v1.

[15] Nomura, W., Yatsui, T., Kawazoe, T., Naruse, M., & Ohtsu, M. (2010). Structural dependency of optical excitation transfer via optical near-field interactions between semiconductor quantum dots. *Appl. Phys. B*, *100*, 181-187

[16] Ohtsu, M. (2019). Indications from dressed photons to macroscopic systems based on hierarchy and autonomy. *Off-shell Archive,* Offshell: 1906R.001.v1.

[17] Naruse, M., Leibnitz, K., Peper, F., Tate, N., Nomura, W., Kawazoe, T., Murata, M., & Ohtsu, M. (2011). Autonomy in excitation transfer via optical near-field interactions and its implications for information networking. *Nano Communication Networks*, *2*, 189-195.

[18] Sangu, S., Kobayashi, K., Shojiguchi, A., & Ohtsu M. (2004). Logic and functional operations using a near-field optically coupled quantum-dot system. *Phys. Rev. B* **69**, 115334.

[19] Shojiguchi, A., Kobayashi, K., Sangu, S., Kitahara, K., & Ohtsu, M. (2003). Superradiance and dipole ordering of an *N* two-level system interacting with optical near fields. *J. Phys. Soc. Jpn.* **72**, 2984-3001.

[20] Kobayashi, K., Sangu, S., Shojiguchi, A., Kawazoe, T., Kitahara, K., & Ohtsu, M. (2003). Excitation dynamics in a three-quantum dot system driven by optical near field interaction: towards a nanometric photonic devices. *J. Microsc.* **210**, 247-251.

[21] Sangu, S., Kobayashi, K., Shojiguchi, A., Kawazoe, T., & Ohtsu, M. (2003). Excitation energy transfer and population dynamics in a quantum dot system induced by optical near-field interaction. *J. Appl. Phys*. **93**, 2937-2945.

[22] Naruse, M., Holmstrom, P., Kawazoe, T., Akahane, K., Yamamoto, N., Thylen, L., & Ohtsu, M. (2012). Energy dissipation in energy transfer mediated by optical near-field interactions and their interfaces with optical far-fields. *Appl. Phys. Lett*., *100*, 241102.

[23] Naruse, M., Tate, N., Aono, M., & Ohtsu, M. (2013). Information physics fundamentals of nanophotonics. *Rep. Prog. Phys.*, *76*, 1-50.

[24] Aono, M., Naruse, M., Kim, S-J., Wakabayashi, M., Hori, H., Ohtsu, M., & Hara, M. (2013). Amoeba-Inspired Nanoarchitectonic Computing: Solving Intractable Computational Problems Using Nanoscale Photoexcitation Transfer Dynamics. *Langmuir*, *29*, 7557-7564.

[25] Naruse, M., Kawazoe, T., Ohta, R., Nomura, W., & Ohtsu, M. (2009). Optimal mixture of randomly dispersed quantum dots for optical excitation transfer via optical near-field interactions. *Phys. Rev. B*, *80*, 125325.

[26] Katori, M. & Kobayashi, H. (2018). Nonequilibrium Statistical Mechanical Models for Photon Breeding Processes Assisted by Dressed-Photon-Phonons. In M. Ohtsu and T. Yatsui (Eds.). *Prog. Nanophotonics 4* (pp.19-55). Heidelberg: Springer.

[27] Tanaka, Y. & Kobayashi, K. (2007). Spatial localization of an optical near field in one-dimensional nanomaterial system. *Physica*, *E40*, 297-300.

[28] Higuchi, Y. & Segawa E. (2009). Dynamical system induced by quantum walks. *J. Phys A: Mathematical and Theoretical* **52**, 395202.

[29] Konno, N., Segawa, E. & Martin Štefa ˇnák, M. (2021). Relation between Quantum Walks with Tails and Quantum Walks with Sinks on Finite Graphs. *Symmetry* **13**, 1169. https://doi.org/10.3390/sym13071169

[30] Higuchi, K., Komatsu, T., Konno, N., Morioka, H. & Segawa, E. (2021). A Discontinuity of the Energy of Quantum Walk in Impurities. *Symmetry* **13**, 1134. https://doi.org/10.3390/sym13071134

Appendix Schematic representations of other modes

This appendix reviews the DP hopping behaviors of the modes presented in Section 5.1 by referring to Figs. 14 and 15.

[Mode **2**] (Fig. A.1)
Figure A.1 schematically explains mode 2, where one arrow arrives at the vertices C and D in Fig. A.1(e). For comparison, two arrows arrive at each vertex of the right triangle in Fig. 15(c). This difference is the reason why mode 2 cannot be used for the QW model, as was pointed out at the end of Section 5.1. Mode 10 cannot be used either due to this difference.

Modes 4, 7, 12, 15, and 18 can be schematically represented in a similar manner to that for mode 1:

[Mode 4] (Fig. A.2)

[Mode 7] (Fig. A.3)

[Mode 12] (Fig. A.4)

[Mode 15] (Fig. A.5)

[Mode 18] (Fig. A.6)

Figure A.7 schematically demonstrates the possibility of transforming mode 1 to modes 4, 7, 12, 15, and 18 by rotating +90 degree two or three times and subsequently inverting the directions of the red and blue arrows *). Due to this possibility, it is confirmed that mode 1 is the representative of the groups, as was described in Section 5.1.

(*) Figure A.7 does not include the mode that can be formed by rotating +90 degree only one time. For reference, the modes formed by such a single rotation are illustrated by Fig. A.8. It is easily found that these modes do not represent the DP hopping and screw-like advancing motion in the forward-upper and backward-lower directions, respectively. This is because the bent red and blue arrows in this figure include the hopping along the -x- and +x-axis, respectively.

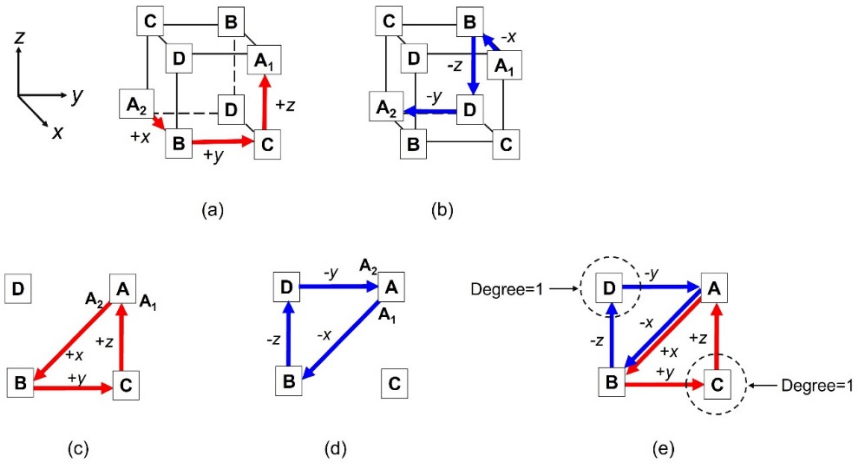

Fig. A.1 Mode 2

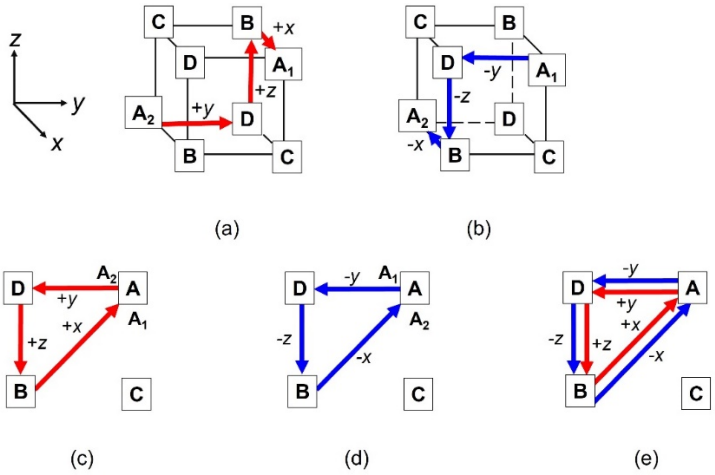

Fig. A.2 Mode 4

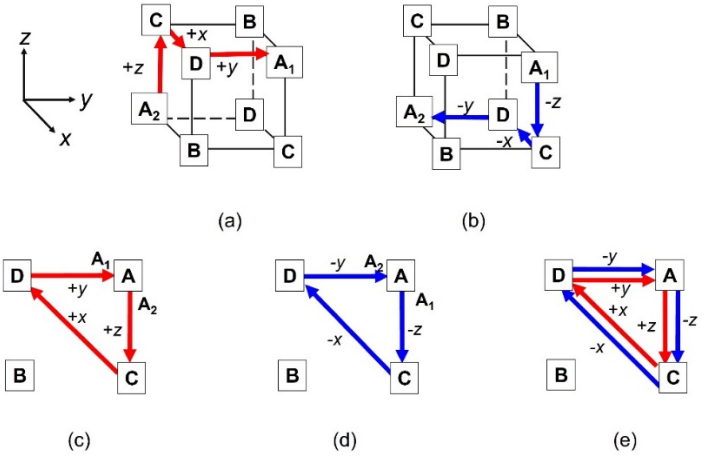

Fig. A.3 Mode 7

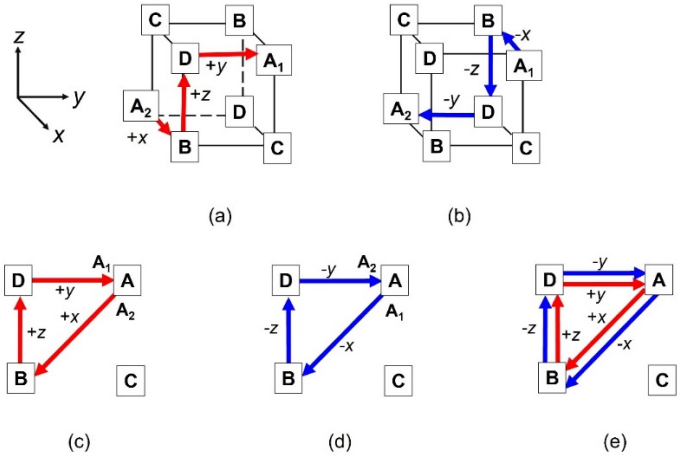

Fig. A.4 Mode 12

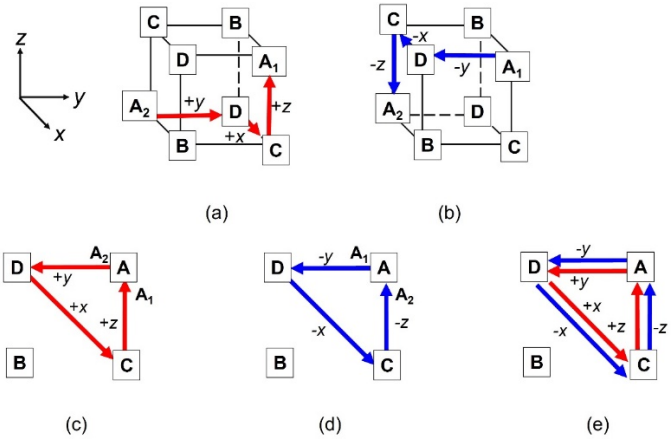

Fig. A.5 Mode 15

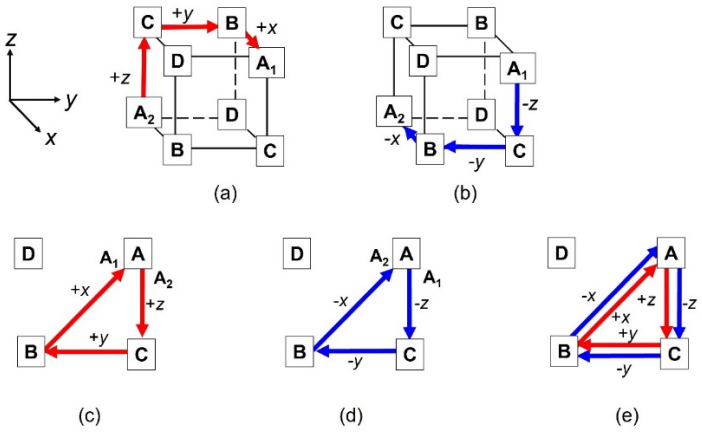

Fig. A.6 Mode 18

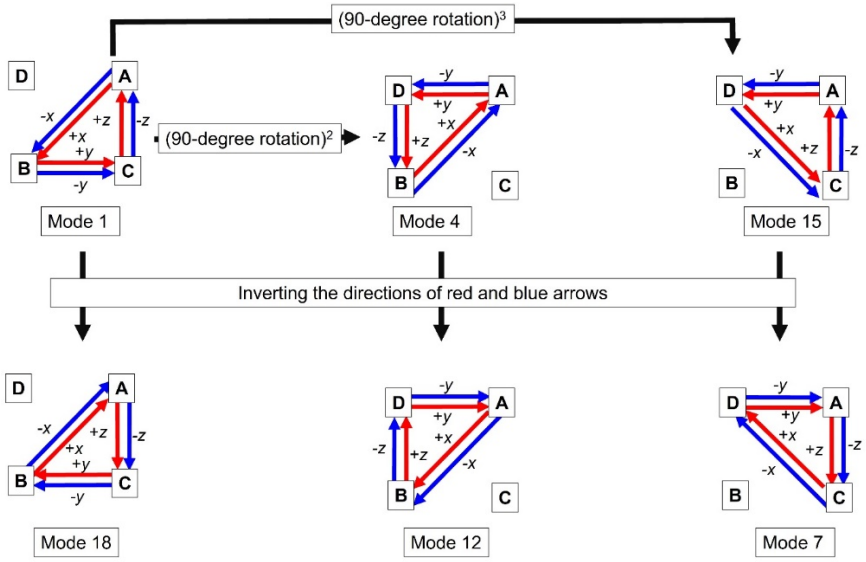

Fig. A.7 Transformation of mode 1 to modes 4, 7, 12, 15, and 18.

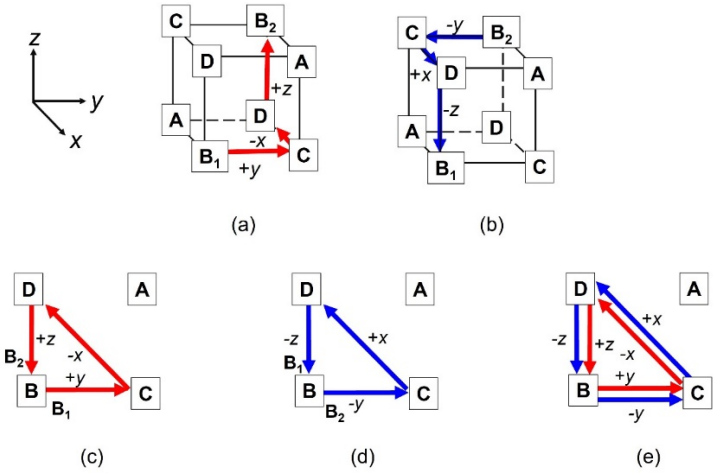

Fig. A.8 The modes formed by rotating +90 degree only one time.